J. Fluid Mech. (2012), *vol.* 711, *pp.* 667–680.
doi:10.1017/jfm.2012.429

A flow in the depth of infinite annular cylindrical cavity

Vladimir Shtern†

Shtern Research and Consulting, Houston, TX 77096, USA

(Received 21 March 2012; revised 15 July 2012; accepted 27 August 2012;
first published online 25 September 2012)

The paper describes an asymptotic flow of a viscous fluid in an infinite annular cylindrical cavity as the distance from the flow source tends to infinity. If the driving flow near the source is axisymmetric then the asymptotic pattern is cellular; otherwise it is typically not. Boundary conditions are derived to match the asymptotic axisymmetric flow with that near the source. For a narrow cavity, the asymptotic solutions for the axisymmetric and three-dimensional flows are obtained analytically. For any gap, the flow is described by a numerical solution of an eigenvalue problem. The least decaying mode corresponds to azimuthal wavenumber $m = 1$.

Key words: low-Reynolds-number flows, separated flows, Stokesian dynamics

1. Introduction

This work extends the studies by Moffatt (1964), Shankar (1998), Hall, Hills & Gilbert (2009) and other researchers to flow in an infinitely deep annular cavity. Moffatt discovered that a flow in a narrow corner between two planes has an infinite number of vortices, whose scale and intensity decrease as the corner edge is approached. An axisymmetric flow between concentric cones has vortices similar to those in Moffatt's problem (Hall, Hills & Gilbert 2007). A motion in a plane infinitely deep cavity (Shankar & Deshpande 2000) can be considered to be a limiting case of that in the corner whose angle tends to zero. The vortex scale does not decrease in the plane cavity, in contrast to the corner and cone flows. Reviews of early studies are in Shankar's book (2007) and the paper by Hall *et al.* (2009).

Cavity flow has been the subject of numerous works motivated by both fundamental and technological interest (Shankar & Deshpande 2000). Among three-dimensional cavities, the cylindrical cavity has attracted the most attention. Elongated cylindrical containers are widely used in several technologies, e.g. vortex tubes, hydrocyclones and vortex combustors (Shtern 2012). A sealed cylinder with one rotating disk serves for fundamental studies of the nature of vortex breakdown (VB) (Escudier 1988). Hills (2001) studied the slow flow in an infinite cylindrical container with a rotating cover. Muite (2004) explored a container flow at small but finite Reynolds numbers. Elongated cylindrical containers are of special interest in recent VB research (Lopez 2012).

† Email address for correspondence: vshtern40@gmail.com

The advantages of confined flows in a cavity with a sliding cover, and in a cylindrical or conical container with a rotating cover, are simple and well-controlled domains and boundary conditions, which allow for meaningful comparisons of experimental and numerical results. Surprisingly, flow in an annular cylindrical cavity has not attracted much attention, in spite of its fundamental and technological relevance.

Our paper addresses this flow and differs from previous studies in terms of (i) cavity geometry, (ii) boundary conditions, (iii) time-dependent flows, and (iv) matching conditions. First, we consider an annular cylindrical cavity. In some vortex combustors, the cylinder is annular; this motivates our study of annular flows. In addition, the annular geometry is generic, encompassing a plane cavity, in the limiting case as the gap-to-radius ratio tends to zero, and a cylindrical container, in the limiting case as the inner-to-outer radius ratio tends to zero.

Second, in contrast to sliding and rotating covers, we consider more general boundary conditions at the cavity end where the flow source is located. The only limitation is the zero flow rate (ZFR), implied by the cavity dead end. Therefore we consider a ZFR flow where the flow rate is zero, e.g. through any cross-section normal to the cavity axis. This condition is valid for a wide variety of flows in addition to those driven by sliding and rotating covers. An example is a flow in a cylindrical container with one end closed. The flow enters and leaves the container through the open end. Such flows model vortex combustors and vortex traps (Shtern, Torregrosa & Herrada 2011*a*,*b*). For small Reynolds number *Re*, a few flow cells exist in elongated cylinders. The number of cells increases with the length-to-radius (aspect) ratio.

At greater depth, a ZFR flow becomes oblivious to most of the constraints posed by boundary conditions at the flow-source end. Even if boundary conditions are steady and axisymmetric, a flow can be time-dependent and three-dimensional due to instability, as has been shown for the container with a rotating end wall (Sorensen, Naumov & Okulov 2011; Lopez 2012). Any ZRF flow decays as the distance from the flow source increases, and eventually becomes so slow that it can be governed by the linear Stokes equations rather than the nonlinear Navier–Stokes equations.

Therefore, the Stokes flow is a limiting case for any ZFR motion as the distance from the flow source tends to infinity. This feature makes the Stokes flow of general interest. The Stokes equations allow for solutions proportional to $\exp(-\lambda z)$, where z is the distance from the flow source and λ must be found as an eigenvalue. In general, λ is a complex number; its real part, λ_r, is a decay rate as z increases.

The asymptotic flow is determined by modes with smallest λ_r. In axisymmetric flows, swirl and meridional motions have different decay rates because the corresponding equations are uncoupled. The axisymmetric asymptotic flow is cellular. In more general flows, swirl and meridional motions are coupled; the asymptotic pattern corresponds to modes with azimuthal wavenumber $m = \pm 1$ and is typically not cellular. This feature of annular cylindrical flow is similar to that in annular conical flows (Hall *et al.* 2009).

Third, we consider time-dependent flow. A flow near the flow source can be time-oscillating or even turbulent. In the cavity depth, such a flow can preserve its unsteady nature even where the flow is very slow. We explore this possibility.

Fourth, we deduce boundary conditions to match near-source and asymptotic axisymmetric flows. These conditions can be used in numerical simulations and allow for a finite-length computational domain, with matching conditions at the end opposite to the flow-source end.

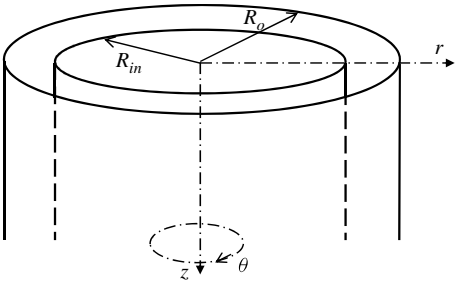

FIGURE 1. Problem geometry.

We start with axisymmetric flow because this particular case is important for combustor and VB applications. For example, the Vogel–Escudier flow is steady and axisymmetric for small Reynolds number Re. As Re exceeds its critical value, Re_{cr}, typically a few thousands, the flow instability results in unsteady and three-dimensional motion. Experiments (Sorensen *et al.* 2011) and simulations (Lopez 2012) indicate that Re_{cr} increases roughly proportionally to the aspect ratio in elongated containers. Therefore the asymptotic steady axisymmetric flow, as the aspect ratio tends to infinity, merits study.

Next, we consider helical modes, $m = \pm 1, \pm 2$ and show that the $m = \pm 1$ mode has the smallest decay rate in a cavity of any gap. The corresponding λ is a real number, except for a very small inner-to-outer radius ratio of the cylindrical sidewalls, and the corresponding flow is typically not cellular.

In the rest of the paper, we formulate the problem (§ 2), analyse the asymptotic axisymmetric (§ 3) and three-dimensional (§ 4) motions, and summarize the results (§ 5).

2. Problem formulation

Consider a flow of a viscous fluid in a semi-infinite annular cavity, $R_{in} < r < R_o$, $0 < z < \infty$, where r and z are the radial and axial cylindrical coordinates (figure 1). Suppose that some non-zero velocity is prescribed at $z = 0$, while the cylindrical sidewalls are still and the cavity terminates at a dead end at $z = \infty$. This implies the zero flow rate (ZFR), e.g. through a cross-section, $z = z_0 \geqslant 0$.

As z increases, a ZFR flow decays and eventually becomes so slow that it can be governed by the linear rather than nonlinear Navier–Stokes equations. We focus here on this asymptotic part of a ZRF flow as $z \to \infty$. Using the gap width $\Delta = R_o - R_{in}$ as a length scale, and Δ^2/ν, ν/Δ, and $\rho\nu^2/\Delta^2$ as scales for time, velocity and pressure, respectively, renders all variables dimensionless; ν is the kinematic viscosity and ρ is the density of the fluid. The Stokes equations can be written in the form (Batchelor 1967)

$$\partial v_r/\partial t + \partial p/\partial r = \nabla^2 v_r - r^{-2} v_r - 2r^{-2}\partial v_\theta/\partial\theta, \tag{2.1a}$$

$$\partial v_\theta/\partial t + r^{-1}\partial p/\partial\theta = \nabla^2 v_\theta - r^{-2} v_\theta + 2r^{-2}\partial v_r/\partial\theta, \tag{2.1b}$$

$$\partial v_z/\partial t + \partial p/\partial z = \nabla^2 v_z, \tag{2.1c}$$

$$\partial v_z/\partial z + \partial v_r/\partial r + v_r/r + r^{-1}\partial v_\theta/\partial\theta = 0, \tag{2.1d}$$

where $\nabla^2 \equiv r^{-1}\partial(r\partial/\partial r)/\partial r + r^{-2}\partial^2/\partial\theta^2 + \partial^2/\partial z^2$, (v_r, v_θ, v_z) are the velocity components in the cylindrical coordinates (r, θ, z), and p is pressure.

Equations (2.1) allow for a solution in the form

$$v_r = U(r)\exp(-\lambda z + \mathrm{i}m\theta + \mathrm{i}\omega t) + \text{c.c.}, \tag{2.2a}$$

$$v_\theta = \mathrm{i}S(r)\exp(-\lambda z + \mathrm{i}m\theta + \mathrm{i}\omega t) + \text{c.c.}, \tag{2.2b}$$

$$v_z = \lambda W(r)\exp(-\lambda z + \mathrm{i}m\theta + \mathrm{i}\omega t) + \text{c.c.}, \tag{2.2c}$$

$$p = P(r)\exp(-\lambda z + \mathrm{i}m\theta + \mathrm{i}\omega t) + \text{c.c.}, \tag{2.2d}$$

where c.c. denotes the complex conjugate of a preceding term.

Any solution of (2.1) can be presented as a linear superposition of modes (2.2) with azimuthal wavenumber $m = 0, \pm1, \pm2, \ldots$ and frequency ω being a real number, $-\infty < \omega < \infty$. For any fixed m and ω, there is a countable set of λ values which must be found. In general, λ is a complex number, $\lambda = \lambda_r + \mathrm{i}\lambda_i$; the subscripts '$r$'and '$i$' indicate real and imaginary parts, respectively. For our problem, eigenvalues with $\lambda_r > 0$ are the only physically relevant ones since the flow decays as z increases. The larger λ_r is, the faster the corresponding mode decays. To explore asymptotic flow features as $z \to \infty$, we focus on modes having small λ_r and therefore decaying more slowly than other modes. These modes provide the main contribution to the asymptotic flow while the contribution of other modes becomes negligible for large z. Due to the linearity of (2.1), each mode can be treated separately.

Substitution of (2.2) reduces (2.1) to ordinary differential equations:

$$S' = S_1/r, \tag{2.3a}$$

$$S_1' = r(a + r^{-2})S - 2mUr^{-1} + mP, \tag{2.3b}$$

$$W' = W_1/r, \tag{2.3c}$$

$$W_1' = r(aW - P), \tag{2.3d}$$

$$P' = \lambda^2 W_1/r + mr^{-2}(S_1 + S) - aU, \tag{2.3e}$$

$$U' = \lambda^2 W - r^{-1}U + mr^{-1}S, \tag{2.3f}$$

where the prime denotes differentiation with respect to r and $a = m^2r^{-2} - \lambda^2 + \mathrm{i}\omega$.

In the gap, $R_{in} \leqslant r \leqslant R_o = R_{in} + 1$, the no-slip boundary conditions at the sidewalls yield

$$W = U = S = 0 \quad \text{at } r = R_{in}, \tag{2.4a}$$

$$W = U = S = 0 \quad \text{at } r = R_o. \tag{2.4b}$$

For the round pipe, where $R_{in} = 0$, the regularity conditions at the axis, $r = 0$, are

$$W_1 = U = S = 0 \quad \text{at } m = 0, \tag{2.5a}$$

$$W = P = U - S = 0 \quad \text{at } m = 1, \tag{2.5b}$$

and

$$W = U = S = 0 \quad \text{at } m \geqslant 2. \tag{2.5c}$$

System (2.3) and the boundary conditions constitute a uniform problem having the trivial (zero) solution. For a non-zero solution, a special (eigen-) value λ is required. In some cases, eigensolutions can be found analytically (see below).

3. Axisymmetric flow

If the prescribed velocity distribution at $z = 0$ is axisymmetric, e.g. corresponding to a rotating disk, the asymptotic flow can be axisymmetric as well. First we consider

this case where $m = 0$ and equations for swirl, (2.3*a*) and (2.3*b*), and meridional motion, (2.3*c*)–(2.3*f*), are uncoupled.

3.1. *Decay of swirl*

To obtain an analytical solution, rewrite (2.3*a*) and (2.3*b*) as the second-order equation

$$S'' = (r^{-2} - \lambda^2 + \mathrm{i}\omega)S - r^{-1}S', \tag{3.1}$$

and address the limiting case as $R_{in} \to \infty$. Then (3.1) is reduced to $S'' + (\lambda^2 - \mathrm{i}\omega)S = 0$ and

$$S = C\sin(n\pi y), \quad y = r - R_{in}, n = 1, 2, \ldots, \tag{3.2a}$$

$$\lambda_r = [n^2\pi^2/2 + (n^4\pi^4 + \omega^2)^{1/2}/2]^{1/2}, \quad \lambda_i = \omega/(2\lambda_r), \tag{3.2b}$$

where C is a constant. Since λ is complex, the flow oscillates with respect to z. The rotation direction (clockwise or anticlockwise) alternates as z varies. The smallest eigenvalue, $\lambda_{sw} = \pi$, corresponding to $n = 1$ and $\omega = 0$, is real; the subscript '*sw*' means 'swirl'. It follows from (3.2*b*) that time-oscillating modes, $\omega \neq 0$, decay more rapidly than steady modes, $\omega = 0$, as z increases.

Next, consider any gap. Introduce $\mu^2 = \lambda^2 - \mathrm{i}\omega$ and note that if μ is a real number then (3.2*b*) is valid, where $n\pi$ is replaced by μ; therefore, time-oscillating modes again decay more rapidly than steady modes for which $\lambda = \mu$. Now we show that the smallest μ is indeed a real number.

To this end, (3.1) is integrated from $y = 0$ to $y = 1$ with the initial conditions $S(0) = 0$ and $S'(0) = 1$. The last condition (normalization) can be used with no loss of generality because the problem is linear and uniform, allowing for an arbitrary constant multiplier. We apply the fourth-order Runge–Kutta procedure with 400 grid points for all numerical simulations reported in this paper. As a result of the integration, $S(1)$ is determined and can be explored as a function of μ, $F(\mu) \equiv S(1)$. The ratio of the gap width to the outer radius is $\delta = 1/R_o$. In the limiting case as $\delta \to 0$, we have $F(\mu) = \sin\mu/\mu$. To find the smallest eigenvalue at any δ in the range $0 < \delta < 1$, we first calculate $F(\mu)$ at $\mu = 0$ and then eventually increase μ. A value of μ at which $F(\mu)$ vanishes is needed.

Figure 2 depicts $\sin\mu/\mu$ (solid curve, $\delta = 0$) and the calculation results for $\delta = 0.5$ and $\delta = 1$. Complex roots can appear only if two real roots merge and disappear. No merging is observed in figure 2. Since the smallest eigenvalues μ are real, time-independent modes decay more slowly than time-oscillating modes, and $\lambda = \mu$ at $\omega = 0$. Figure 3 depicts the dependence of the smallest $\lambda = \lambda_{sw}$ on δ. As δ increases from 0 to 1, λ_{sw} increases from 3.1416 to 3.8317. At $\delta = 1$, our results for the steady swirl agree with those obtained by Hills (2001) for the cylindrical container with a rotating end wall.

Figure 4 depicts the asymptotic profile of swirl velocity. Under the normalization, $v_{\theta max} = 1$, the profile is nearly invariant as δ varies from 0 to 1, e.g. the maximum velocity location shifts from $y = 0.5$ to $y = 0.48$. Recall that the swirling mode does not involve the meridional motion. In the limiting case as $\delta \to 0$, the velocity of corresponding flow in a plane cavity is parallel to its sidewalls and plane, $z = 0$. Note that large eigenvalues of μ are close to $n\pi, n \gg 1$, because the terms, $r^{-2}S$ and $r^{-1}S'$, in (3.1) become negligible compared with the other terms and therefore (3.1) is reduced to $S'' + \mu^2 S = 0$.

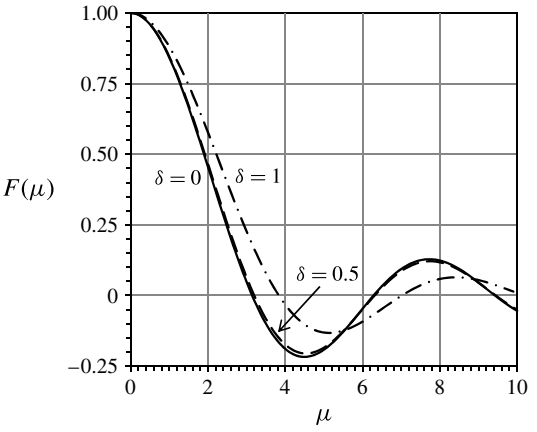

FIGURE 2. $F(\mu)$ is zero at an eigenvalue μ: solid curve, $\delta = 0$; dashed curve, $\delta = 0.5$; dot-dashed curve, $\delta = 1$.

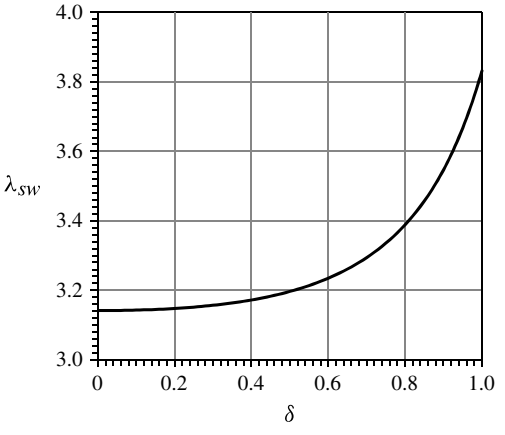

FIGURE 3. Dependence of the smallest decay rate of swirl, λ_{sw}, on gap/(outer radius) ratio δ.

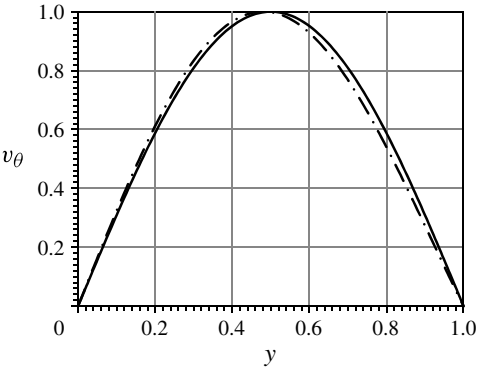

FIGURE 4. Swirl velocity profiles for a small gap ($\sin(\pi y)$, solid curve) and for a round pipe (dot-dashed curve).

3.2. *Decay of meridional motion*

Small gap

For analytical calculations, it is convenient to use the Stokes stream function

$$\Psi = \lambda Q(r)\exp(-\lambda z + \mathrm{i}m\theta + \mathrm{i}\omega t) + \text{c.c.}, \quad v_z = r^{-1}\partial\Psi/\partial r, \quad v_r = -r^{-1}\partial\Psi/\partial z. \tag{3.3}$$

Then, in the limiting case as $\delta \to 0$, the equations describing the meridional motion can be reduced to

$$Q'''' + (\lambda^2 + \mu^2)Q'' + \lambda^2\mu^2 Q = 0. \tag{3.4}$$

Its solution, $Q(y)$, satisfying the no-slip conditions, $Q(0) = Q'(0) = Q(1) = 0$, is

$$\begin{aligned} Q = C\{&(\cos\mu - \cos\lambda)[\lambda\sin(\mu y) - \mu\sin(\lambda y)] \\ &- (\lambda\sin\mu - \mu\sin\lambda)[\cos(\mu y) - \cos(\lambda y)]\}, \end{aligned} \tag{3.5}$$

where C is a constant, which can be conveniently chosen to satisfy a normalization condition, e.g. $Q(0.5) = 1$. The no-slip condition, $Q'(1) = 0$, yields that

$$F(\lambda) \equiv C[2\lambda\mu(1 - \cos\mu\cos\lambda) - (\lambda^2 + \mu^2)\sin\lambda\sin\mu] = 0. \tag{3.6}$$

At $\omega = 0$, the smallest eigenvalue is $\lambda_m = 4.212 + \mathrm{i}2.251$, which agrees with the known value obtained for the plane cavity flow (Shankar & Deshpande 2000). As ω increases, λ_{mr} also increases, e.g. $\lambda_m = 4.493 + i2.742$ at $\omega = 10$. This feature is valid for any gap according to our numerical simulations at $\omega = 10$ as δ increases from 0 to 1. Since steady meridional modes decay more slowly than time-oscillating ones, like the swirl case, we now address only steady axisymmetric modes.

Moderate gap

Now consider an annular pipe with an arbitrary gap. A solution can be represented in terms of Bessel functions (Shankar 1997), but we have found that direct numerical simulations are less laborious. To numerically solve the eigenvalue problem for the meridional motion, (2.3*c*)–(2.3*f*) are integrated from $y = 0$ to $y = 1$ with initial conditions $W = U = 0, P = 1$ (normalization) and $W_1 = W1$ at $y = 0$. A value of $W1$ is found by 'shooting' to satisfy the condition $W(1) = 0$. Since the problem is linear, shooting rapidly converges for any initial guess for $W1$. As a result, $U(1)$ is determined and explored as a function λ, $F(\lambda) \equiv U(1)$. Figure 5 depicts contours $F_r = 0$ and $F_i = 0$ on the complex plane (λ_r, λ_i) for $\delta \ll 1$, $\delta = 0.5$ and $\delta = 1$. Only the region where $\lambda_r > 0$ and $\lambda_i > 0$ is shown, because both the abscissa and the ordinate are lines of symmetry. According to system (2.3) at $\omega = 0$, if λ is an eigenvalue, then eigenvalues are $-\lambda$, λ^* and $-\lambda^*$ as well; the symbol '$*$' denotes the complex conjugate.

At points where the solid curves intersect the abscissa in figure 5, pole singularities are located. Therefore, figure 5 reveals no real eigenvalue λ. Complex λ means a cellular axisymmetric motion. Figure 6 depicts streamline patterns corresponding to the minimal decay rate for $\delta \ll 1$, $\delta = 0.5$ and $\delta = 1$. Figure 7 depicts the dependence of the smallest λ_{mr} and related λ_{mi} on the gap width; index 'm' denotes the meridional motion. Since $r = 0$ is a singularity point for system (2.3), we terminate integration as R_{in} decreases down to 0.0001, where $\lambda_m = 4.482 + \mathrm{i}1.6617$. With the no-slip conditions at $r = R_{in}$, a singularity develops in the limiting case as $R_{in} \to 0$. This explains the character of the curve near the ordinate in figure 7.

For transition to the round-pipe flow, we must replace conditions (2.4*a*) by (2.5*a*), because in a round pipe (i) the axial velocity, W, is not zero at the axis, and (ii) the regularity requires that $W_1 = 0$ at $r = 0$. The new boundary conditions yield

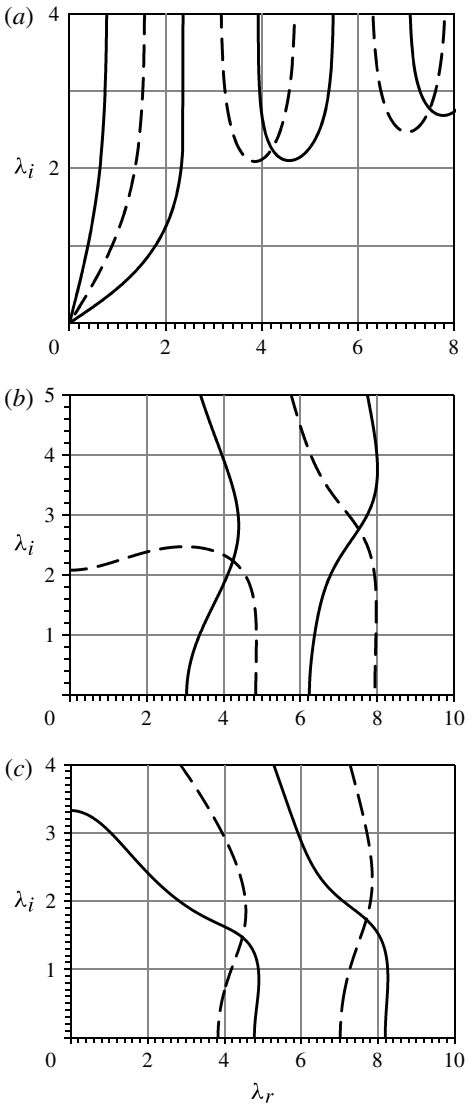

FIGURE 5. Contours $F_r = 0$ (solid curves) and $F_i = 0$ (dashed curves) for (a) a small gap, $\delta \ll 1$, (b) $\delta = 0.5$, and (c) a round pipe, $\delta = 1$.

$\lambda_m = 4.466 + \mathrm{i}1.4675$, which agrees with the first eigenvalue found by Shankar (1998). The difference between the results for the annular and round pipes is small for λ_{mr} but remarkably large for λ_{mi}.

3.3. *Matching conditions*

The asymptotic solution obtained allows us to derive conditions to match the above described large-z flow with that occurring for small and moderate z. Here we derive the matching conditions for a steady axisymmetric flow. For the swirl velocity, the condition is straightforward:

$$\partial v_\theta / \partial z + \lambda_{sw} v_\theta = 0. \tag{3.7}$$

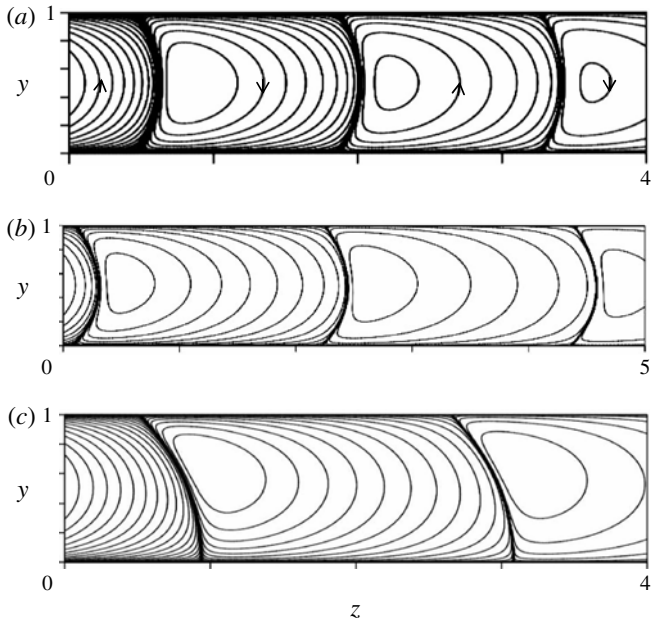

FIGURE 6. Streamlines for (*a*) a small gap, $\delta \ll 1$, (*b*) $\delta = 0.5$, and (*c*) a round pipe, $\delta = 1$.

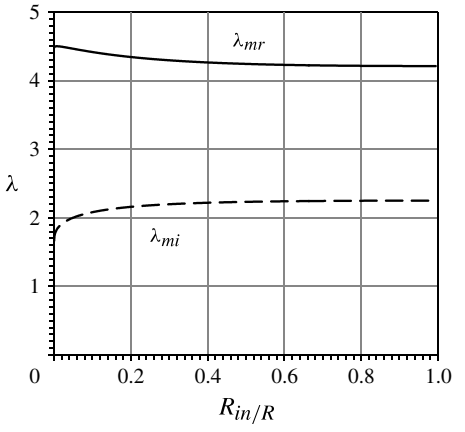

FIGURE 7. Decay rate of meridional flow in an annular pipe: solid curve, λ_{mr}; dashed curve, λ_{mi}. The gap width serves as a length scale for λ_m.

For the meridional motion, we apply the solution for the Stokes stream function in the form

$$\Psi = Q(r)\exp(-\lambda_m z) + Q^*(r)\exp(-\lambda_m^* z), \tag{3.8}$$

where the symbol '$*$' denotes the complex conjugate. Differentiating (3.8) three times with respect to z and excluding $Q(r)\exp(-\lambda_m z)$ and $Q^*(r)\exp(-\lambda_m^* z)$ yields the conditions

$$\partial^2\Psi/\partial z^2 + 2\lambda_{mr}\partial\Psi/\partial z + (\lambda_{mr}^2 + \lambda_{mi}^2)\Psi = 0, \tag{3.9a}$$

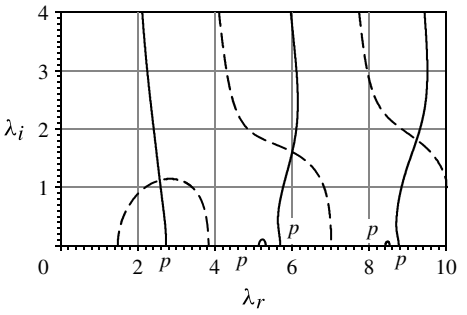

FIGURE 8. Contours $F_r = 0$ (solid curves) and $F_i = 0$ (dashed curves) for a round pipe, $\delta = 1, m = 1$.

$$\partial^3\Psi/\partial z^3 + (\lambda_{mi}^2 - 3\lambda_{mr}^2)\partial\Psi/\partial z - 2\lambda_{mr}(\lambda_{mr}^2 + \lambda_{mi}^2)\Psi = 0. \tag{3.9b}$$

Conditions (3.7) and (3.9) can be applied at a sufficiently large z for any ZFR flow in a semi-infinite pipe. They can help reduce the domain of numerical simulations. Conditions (3.7) and (3.9) can be applied for any gap value as well as for the round pipe.

We conclude that the asymptotic axisymmetric flows in the annular and round cavities are similar. The common features are (i) the cellular character of the meridional motion, and (ii) that the swirl decays more slowly than meridional flow as z increases. In contrast, the asymptotic three-dimensional flows in annular and round cavities are very different, as shown below.

4. Steady three-dimensional flow

4.1. *Cylindrical cavity*

For comparison, we first re-examine the steady flow in the cylindrical cavity. Shankar (1998) found that the smallest decay rate corresponds to the $m = 1$ mode with $\lambda_{1c} = 2.5678 + \mathrm{i}1.122$; the subscripts 1 and '$c$' indicate the $m = 1$ mode and the cylindrical cavity, respectively.

To find eigenvalues we integrate (2.3) from $y = 1$ with initial conditions $W = U = S = 0, P = 1$ (normalization), $W_1 = W1$ and $S_1 = S1$. To avoid the singularity at $y = 0$, the integration terminates at $y_f = 0.0001$. Values of $W1$ and $S1$ are found by shooting to satisfy the conditions $W = 0$ and $U = S$ at $y = y_f$: see (2.5*b*). As the problem is linear, shooting rapidly converges from any guess. As a result, $P(y_f)$ is determined, which is explored as a function λ, $F(\lambda) \equiv P(y_f)$. Points where $F(\lambda) = 0$ correspond to eigenvalues.

Figure 8 depicts contours $F_r = 0$ and $F_i = 0$ on the complex plane (λ_r, λ_i). The symbol 'p' indicates singularities which are poles. Figure 8 reveals three complex and two real eigenvalues. These values agree with those found by Shankar (1998) to five significant figures.

The difference is in flow patterns. Shankar addressed a flow induced by a sliding cover. This flow has a plane of symmetry, $\theta = \text{const}$. In contrast, we consider a ZFR flow which typically has no plane of symmetry. The problem is invariant with respect to the transformation, $(m, v_\theta) \to (-m, -v_\theta)$. Let $\boldsymbol{v}_1$ and $\boldsymbol{v}_{-1}$ be solutions for $m = 1$ and $m = -1$ respectively (with the same λ). A general solution is $\boldsymbol{v} = C_1\boldsymbol{v}_1 + C_{-1}\boldsymbol{v}_{-1}$, where C_1 and C_{-1} are constants. The plane of symmetry exists at $C_1 = C_{-1}$. In this

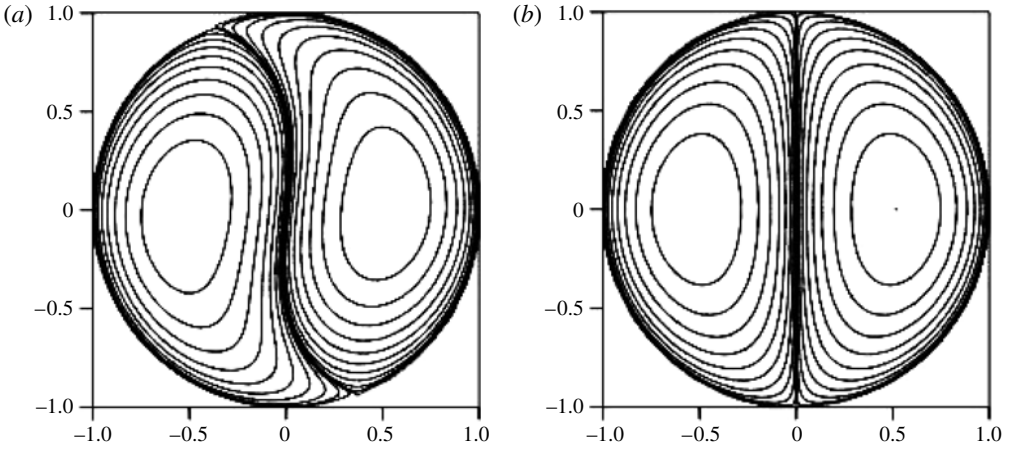

FIGURE 9. Contours $v_z = \text{const.}$ at a fixed z for (a) helical modes ($C_1 = 0$ or $C_{-1} = 0$) and (b) symmetric modes ($C_1 = C_{-1}$), corresponding to the smallest decay rate in a cylindrical cavity.

case, the asymptotic flow is cellular, but it is not for $C_1 \neq C_{-1}$. Figure 9 depicts contours $v_z = \text{const.}$ at a fixed z for helical ($C_1 = 0$ or $C_{-1} = 0$) and symmetric modes ($C_1 = C_{-1}$) at $\lambda = \lambda_{1c}$. Let the left-hand (right-hand) side correspond to positive (negative) v_z. At the separating curves and the sidewall (bold lines), the axial velocity is zero.

Figure 9(a) rotates clockwise (for $\boldsymbol{v}_{-1}$) or anticlockwise (for $\boldsymbol{v}_1$) while figure 9(b) is invariant as z increases. The other velocity components behave similarly. The regions of positive and negative v_z as well as the separating surface are helical and unbounded for the flow corresponding to figure 9(a). Therefore, this flow is not cellular. In contrast, the flow corresponding to figure 9(b) is cellular (Shankar 1998).

4.2. *Annular cavity*

As in the case of axisymmetric modes, there is no continuous transition from the round to annual cavity for $m = 1$ modes because the no-slip (2.4a) and regularity (2.5b) conditions differ. With the no-slip condition at $y = y_f$, we found that $\lambda_1 = 2.76 + \mathrm{i}0.78$. Comparison of λ_1 and λ_{1c} shows that the no-slip condition yields more rapid flow decay as z increases, and a larger wavelength in the z direction, than does the regularity condition. This trend becomes even more prominent as δ decreases.

Figure 10 depicts the dependence of the smallest λ_r and the corresponding λ_i on the gap width δ for a few leading modes: $m = 0$, 1 and 2. Figure 10(b) is a close-up of the vicinity of $\delta = 1$. The numbers near the curves are m values. Note that the transition from the round to annular cavity is continuous for the $m = 2$ mode, because the no-slip and regularity conditions agree for $m \geqslant 2$.

The striking effect is that the complex λ merges with its complex conjugate and transforms into two real eigenvalues as δ decreases for both $m = 1$ and 2. This metamorphosis occurs at δ close to 0.993 (0.81) for $m = 1$ ($m = 2$). The smaller (larger) real λ tends to 0 (π) as $\delta \to 0$. The mode corresponding to the larger real λ tends as $\delta \to 0$ to the flow described by analytical solution (3.2) at $n = 1$. The

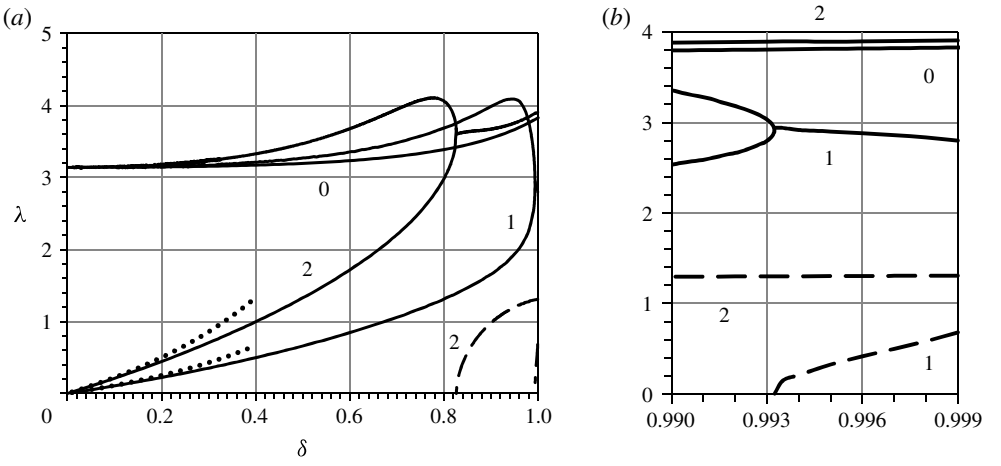

FIGURE 10. (*a*) Dependence of decay rate λ_r (solid curves) and wavenumber λ_i (dashed curves) on gap δ. The numbers near the curves are m values. (*b*) Close-up of the vicinity of $\delta = 1$. The dotted curves are asymptotes, $\lambda = m\delta/(1-\delta)$, as $\delta \to 0$.

mode corresponding to the smaller real λ tends as $\delta \to 0$ to the flow described by the analytical solution derived below.

4.3. *Analytical solution for azimuthal modes in a narrow annular cavity*

In the limiting case as $\delta \to 0$, the annular cavity tends to the plane cavity and the azimuthal coordinate θ can be replaced by $x = \theta R_{in}$. Let $\theta \to 0$ as $R_{in} \to \infty$, so that the limiting value of x is finite. The Stokes equations in Cartesian coordinates (x, y, z) have the solution

$$v_x = p_0 \alpha W \sin(\alpha x)\exp(-\alpha z), \quad v_y = 0, \quad v_z = p_0 \alpha W \cos(\alpha x)\exp(-\alpha z), \quad (4.1a)$$

$$p = 8p_0 \cos(\alpha x)\exp(-\alpha z), \quad \Psi_{az} = p_0 W \sin(\alpha x)\exp(-\alpha z), \quad W = 4y(1-y). \quad (4.1b)$$

Here p_0 is a constant, α is a wavenumber of x-oscillations, $\lambda = \alpha$ is the decay rate in the z direction, Ψ_{az} is the stream function, $v_z = \partial\Psi_{az}/\partial x$ and $v_x = -\partial\Psi_{az}/\partial z$, and the y-profile, W, is normalized to its maximum, $W(0.5) = 1$; the subscript 'az' means azimuthal.

Solution (4.1) describes a flow which is parallel to the cavity sidewalls, periodic along the cavity, and which decays in the cavity depth as $z \to \infty$. The decay rate can be arbitrarily small for $\alpha \to 0$, but solution (4.1) becomes trivial at $\alpha = 0$, so that $\lambda = 0$ is not an eigenvalue. Figure 11 depicts streamlines, $\Psi_{az} = \text{const.}$, corresponding to solution (4.1) in the cross-section $y = 0.5$ (the pattern is similar for any y), and shows one period in the x direction.

To describe this mode in the annular cavity of large $R_{in} = 1/\delta - 1$, we substitute $x = \theta R_{in}$. Now $\alpha = m/R_{in} = m\delta/(1-\delta)$ has only discrete values corresponding to $m = 1, 2, \ldots$. Accordingly, the decay rate is $\lambda = m\delta/(1-\delta)$ (the dotted curves in figure 10), which explains the asymptotic behaviour of the curves labelled 1 and 2 in figure 10 as $\delta \to 0$.

Figure 12 depicts profiles of the axial (W), swirl (S), and radial (U) velocities at $m = 1$, $\lambda = 1.66$ and $\delta = 0.9$ (see the curve labelled 1 in figure 10). For comparison, the analytical solution, $W_a = 4y(1-y)$ as $\delta \to 0$, is also shown. Even for this small $R_{in} = 1/9$, the profiles W and W_a are close, and the radial velocity is small compared

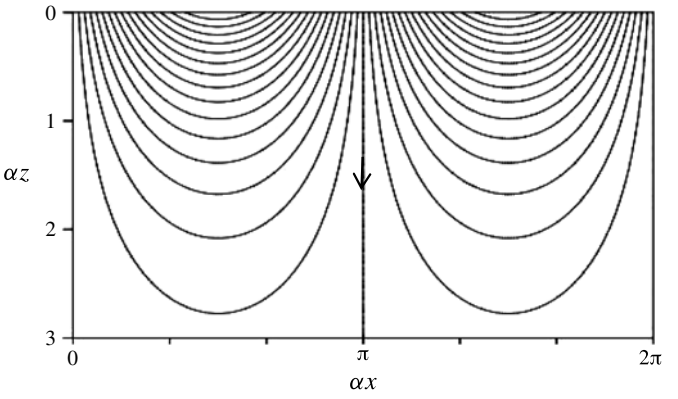

FIGURE 11. Streamlines of a plane flow parallel to the sidewalls of a plane cavity.

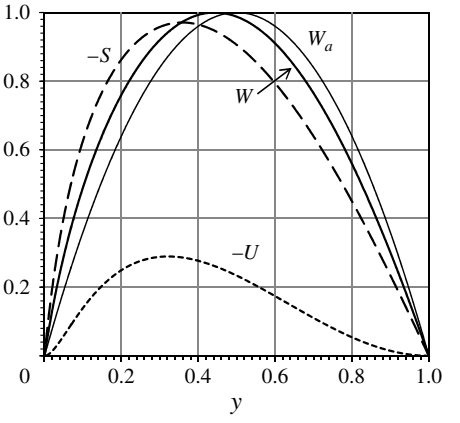

FIGURE 12. Profiles of the axial (W, bold curve), swirl (S, dashed curve) and radial (U, dotted curve) velocities at $m = 1$, $\lambda = 1.66$ and $\delta = 0.9$; $W_a = 4y(1 - y)$ (thin solid curve) is the profile of W and $-S$ as $\delta \to 0$.

with the axial and swirl velocities, i.e. the numerical results for $\delta = 0.9$ and the analytical results as $\delta \to 0$ are rather close.

5. Conclusions

The paper describes the asymptotic pattern of a ZFR flow of a viscous fluid in an annular cylindrical cavity as the distance z from the flow source tends to infinity. The pattern depends on a driving flow.

If the driving flow is axisymmetric, the asymptotic pattern is cellular and the number of vortices is infinite in the cavity depth. In the limiting cases of the narrow gap and the round cavity, our results agree with earlier ones (Shankar & Deshpande 2000; Hills 2001). It is shown that time-oscillating axisymmetric modes decay more rapidly than steady modes. Conditions are derived which match the asymptotic and near-surface axisymmetric flows.

If the driving flow is three-dimensional, the asymptotic pattern is typically not cellular. The least decaying mode corresponds to azimuthal wavenumber $m = 1$. The flow monotonically decays as z increases except for inner-to-outer radius ratio less than 0.007. The presence of an inner cylinder radically changes the asymptotic flow, which becomes monotonic with respect to z in contrast to the z-oscillating flow in the cylindrical cavity. Our numerical results are verified by comparison with analytical solutions derived for both axisymmetric and three-dimensional flows in the cavity, with inner-to-outer radius ratio close to 1.

REFERENCES

BATCHELOR, G. K. 1967 *An Introduction to Fluid Dynamics*. Cambridge University Press.

ESCUDIER, M. P. 1988 Vortex breakdown: observations and explanations. *Prog. Aerosp. Sci.* **25**, 189–229.

HALL, O., HILLS, C. P. & GILBERT, A. D. 2007 Slow flow between concentric cones. *Q. J. Mech. Appl. Math.* **60**, 27–48.

HALL, O, HILLS, C. P. & GILBERT, A. D. 2009 Non-axisymmetric Stokes flow between concentric cones. *Q. J. Mech. Appl. Math.* **62**, 137–148.

HILLS, C. P. 2001 Eddies induced in cylindrical containers by a rotating end wall. *Phys. Fluids* **13**, 2279–2286.

LOPEZ, J. M. 2012 Three-dimensional swirling flow in a tall cylinder driven by a rotating endwall. *Phys. Fluids* **24**, 014101.

MOFFATT, H. K. 1964 Viscous and resistive eddies near a sharp corner. *J. Fluid Mech.* **18**, 1–18.

MUITE, B. K. 2004 The flow in a cylindrical container with a rotating end wall at small but finite Reynolds number. *Phys. Fluids* **16**, 3614–3626.

SHANKAR, P. N. 1997 Three-dimensional eddy structure in a cylindrical container. *J. Fluid Mech.* **342**, 97–118.

SHANKAR, P. N. 1998 Three-dimensional Stokes flow in a cylindrical container. *Phys. Fluids* **10**, 540–549.

SHANKAR, P. N. 2007 *Slow Viscous Flows*. Imperial College Press.

SHANKAR, P. N. & DESHPANDE, M. D. 2000 Fluid mechanics in the driven cavity. *Annu. Rev. Fluid Mech.* **32**, 93–136.

SHTERN, V. 2012 *Counterflows*. Cambridge University Press (in press).

SHTERN, V. N., TORREGROSA, M. M. & HERRADA, M. A. 2011*a* Development of a swirling double counterflow. *Phys. Rev.* E **83**, 056322.

SHTERN, V. N., TORREGROSA, M. M. & HERRADA, M. A. 2011*b* Development of colliding counterflows. *Phys. Rev.* E **84**, 046306.

SORENSEN, J. N., NAUMOV, I. V. & OKULOV, V. L. 2011 Multiple helical modes of vortex breakdown. *J. Fluid Mech.* **683**, 430–441.